

# Novel Approach to $^{93m}\text{Mo}$ Isomer Depletion: Nuclear Excitation by Electron Capture in Resonant Transfer Process

J. Rzadkiewicz<sup>1</sup>\*


*National Centre for Nuclear Research, 05-400 Otwock, Poland*

M. Polasik<sup>2</sup>, K. Słabkowska, and Ł. Syrocki<sup>2</sup>

*Faculty of Chemistry, Nicolaus Copernicus University in Toruń, 87-100 Toruń, Poland*

J. J. Carroll<sup>3</sup> and C. J. Chiara<sup>3</sup>

*DEVCOM Army Research Laboratory, Adelphi, Maryland 20783, USA*

 (Received 16 November 2020; revised 26 February 2021; accepted 12 May 2021; published 21 July 2021)

A novel approach for isomer depletion in ion-atom collisions is proposed and considered theoretically. Analyses are performed for the depletion of the  $^{93m}\text{Mo}$  isomer for which an unexpectedly large probability was measured in the beam-based experiment of Chiara *et al.* [*Nature (London)* **554**, 216 (2018)]. The subsequent attempt at a theoretical description based on state-of-the-art atomic theory did not reproduce the experimental result [Wu *et al.*, *Phys. Rev. Lett.* **122**, 212501 (2019)] and showed a dramatic disagreement with the experiment (by many orders of magnitude). This conflict calls for further research on the nature of isomer depletion mechanisms occurring in atomic processes. Here, we propose to consider the  $^{93m}\text{Mo}$  isomer depletion as the nuclear excitation by electron capture in resonant transfer process taking into account the momentum distribution of the target electrons. Although our results only slightly shift the upper theoretical limit for the total  $^{93m}\text{Mo}$  isomer depletion probability toward the experimental value, they show the importance of considering the Compton profile in the theoretical description, in particular for the  $L$  shell, for which the depletion probability increases by many orders of magnitude.

DOI: [10.1103/PhysRevLett.127.042501](https://doi.org/10.1103/PhysRevLett.127.042501)

Nuclear isomers can be characterized as excited nuclear states having reduced wave-function overlap with lower-lying states. This inhibits their decay and, consequently, results in their metastability [1]. Probing the properties of isomers makes possible, for example, improved insight into exotic nuclear structures, discovery of highly deformed nuclear shapes, and the study of correlated fermion motions in the atomic nucleus. Isomers can also significantly change the effective half-life of nuclei in astrophysical plasmas and thus modify their abundances in the stellar environment [2–4].

In recent years, isomers have been considered as energy storage materials [5,6]. The use of isomers for efficient energy storage requires effective methods for isomer production and advanced understanding of the mechanisms that release their energy on demand. Studies of isomer depletion have involved photoabsorption, Coulomb excitation, or thermal neutron capture (see Ref. [7] and references therein), or atomic processes related to the electron-nucleus interaction [8,9].

One such mechanism, which may provide energy release on demand, is nuclear excitation by electron capture (NEEC). NEEC is the inverse process of nuclear internal conversion, and is an analog of atomic dielectronic recombination (DR), with the role of the atomic excitation being

replaced by nuclear excitation. NEEC occurs when a free electron recombines into an unfilled atomic shell of the ion at the resonance energy and the energy released from the capture excites the nucleus.

Inverse internal conversion was originally suggested for the excitation of the  $^{235}\text{U}$  nucleus by the capture of electrons from a laser plasma [10]. Since then, considerable effort has been made to achieve an experimental demonstration of NEEC and its theoretical description [8]. Such investigations of NEEC included scenarios for laser plasmas [11–14], electron beam ion trap [15], storage ring [16,17], ions channeling in crystals [18–20], and beam-based scenarios [21–25].

Of those scenarios, to date only the beam-based one has resulted in an experimental demonstration of NEEC, resulting in depletion [26] of the  $^{93m}\text{Mo}$  isomer at 2425 keV ( $21/2^+$ ,  $T_{1/2} = 6.85$  h) [27]. In the experiment [26], the 9.33-MeV/u  $^{90}\text{Zr}$  ion beam interacted with the  $^7\text{Li}$  target and produced the secondary beam (recoil ions) containing high-spin  $^{93}\text{Mo}$  nuclei feeding the isomer as the ions approached the second target  $^{12}\text{C}$ . The depletion, attributed to NEEC occurring in the  $^{12}\text{C}$  target, was confirmed by detailed analysis of coincidence relationships between  $\gamma$ -ray transitions directly feeding the  $^{93m}\text{Mo}$  isomer and those originating from the isomer excitation into the

17/2<sup>+</sup> depletion state (DS) and its subsequent decay to the ground state [26]. Moreover, the experiment showed an unexpectedly high probability of the <sup>93m</sup>Mo isomer depletion of 0.010(3) across the <sup>12</sup>C target [26].

Wu *et al.*, [28] performed a theoretical analysis of the NEEC probability for the <sup>93m</sup>Mo isomer depletion using state-of-the-art atomic models. Their results showed that a probability in the range of 2.3–2.7 × 10<sup>-11</sup> is in striking disagreement with the experiment. This motivates further research on the nature of the isomer depletion in the beam-based conditions.

In this Letter, we propose a novel theoretical approach describing the depletion of the <sup>93m</sup>Mo isomer in the beam-based conditions. The approach, to the best of our knowledge, is the first profound attempt including the effect of electron binding in target atoms on depletion of the <sup>93m</sup>Mo isomer as a result of the NEEC in resonant transfer (RT). NEEC-RT can be considered as analogous to the atomic resonant electron transfer and excitation (RTE) leading to the formation of innershell excited states [29–32]. The only difference between NEEC-RT and NEEC (as with the difference between atomic processes RTE and DR) is the initial state of the target electron. In NEEC-RT, the ion captures an initially bound electron, while in NEEC, the electron is unbound. The inclusion of weakly bound electrons instead of free electrons has fundamental implications that are related not only to the change of the cross sections, but also to the change in the nature of the process from a quasidiscrete to a continuous one as a function of the projectile energy. This is due to a huge energy broadening of the resonance as a result of the large momentum distribution (Compton profile) of the target electrons in the projectile frame. Moreover, in the NEEC-RT process, one can expect a resonance shift toward higher projectile energies due to the binding energy of target electrons.

In the case of the <sup>93m</sup>Mo ion interacting with a solid <sup>12</sup>C target, the electron can be resonantly transferred from the <sup>12</sup>C target atom into the *L*, *M*, and *N* shells (or higher) of the highly ionized <sup>93m</sup>Mo projectile. The electron transfer can simultaneously excite the isomeric state (IS) into the 17/2<sup>+</sup> DS lying 4.85 keV above. The DS can subsequently decay to the 5/2<sup>+</sup> ground state through a cascade, including the 13/2<sup>+</sup> first intermediate state (FS). A schematic representation of the NEEC-RT process in the <sup>93m</sup>Mo isomer is shown in Fig. 1.

It was shown that RTE is related to DR through the Compton profile of electrons in atomic targets [29–32]. In analogy to RTE and DR, one can obtain the NEEC-RT cross section from the relationship between NEEC-RT and NEEC (treated as pure recombination process) within the impulse approximation (IA) [33]. The approximation assumes the sudden ion-target atom interaction. The assumption is met if the velocity of the projectile is much greater than the orbital velocity of the target electron. As shown for RTE [33], under such collision conditions one

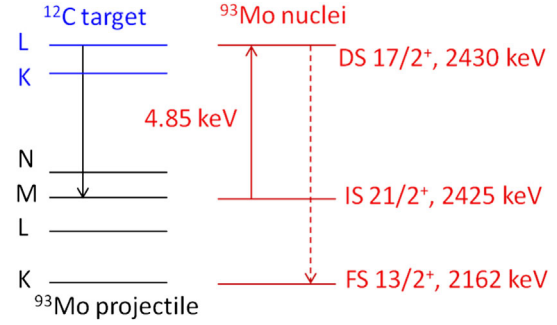


FIG. 1. Schematic representation of the NEEC-RT process. Energies are not to scale.

can also assume that the target electrons are characterized by their momentum distribution, and they populate a continuous distribution of energies in the rest frame of the projectile. This opens up the possibility of applying the IA for the description of the NEEC-RT process. Thus, the NEEC-RT cross sections were derived from the relationship with the recombination NEEC resonance strengths  $S_{\text{NEEC}}^{q,nl_j}$ :

$$\sigma_{\text{NEEC-RT}}^{q,nl_j} = \sum_i \sqrt{\frac{M_p}{2E_p}} J_i(Q) S_{\text{NEEC}}^{q,nl_j}, \quad (1)$$

where  $M_p$  is the mass of the <sup>93m</sup>Mo ion with energy  $E_p$ ,  $J_i(Q)$  is the Compton profile of the <sup>12</sup>C target electrons ( $i = 1s_{1/2}, 2s_{1/2}, \text{ and } 2p_{1/2}$ ), and  $Q$  is the momentum component of the target electron along the direction of the incident projectile.

The estimation of the resonance strength for NEEC occurring in the <sup>93</sup>Mo nucleus was based on the approach originally presented in Ref. [11] and developed in [8,23]. The NEEC resonance strength for a given atomic state  $nl_j$  of the <sup>93m</sup>Mo ion—that is, the integral of the NEEC cross sections over incident electron energies—can be expressed as

$$S_{\text{NEEC}}^{q,nl_j} = g \frac{\lambda_e^2 \alpha_{\text{IC}}^{q,nl_j}(\text{DS} \rightarrow \text{IS}) \Gamma_\gamma(\text{DS} \rightarrow \text{IS})}{4 \Gamma_{\text{tot}}(\text{DS})} \times [1 + \alpha_{\text{IC}}^{q=0}(\text{DS} \rightarrow \text{FS})] \Gamma_\gamma(\text{DS} \rightarrow \text{FS}), \quad (2)$$

where  $\lambda_e$  is the wavelength of the capture electrons with the relative kinetic energy required for NEEC to occur, the factor  $g$  is a function of the nuclear spins and the total angular momentum of the captured electron,  $\alpha_{\text{IC}}^{q,nl_j}(\text{DS} \rightarrow \text{IS})$  are the partial internal conversion coefficients (ICC) for the  $nl_j$  subshell and charge state  $q$ , while  $\alpha_{\text{IC}}^{q=0}(\text{DS} \rightarrow \text{FS})$  is the total ICC. The  $\Gamma_\gamma(\text{DS} \rightarrow \text{IS})$  and  $\Gamma_\gamma(\text{DS} \rightarrow \text{FS})$  are radiative widths and correspond to the intensities of the  $\gamma$  transitions from the DS, and  $\Gamma_{\text{tot}}(\text{DS})$  is

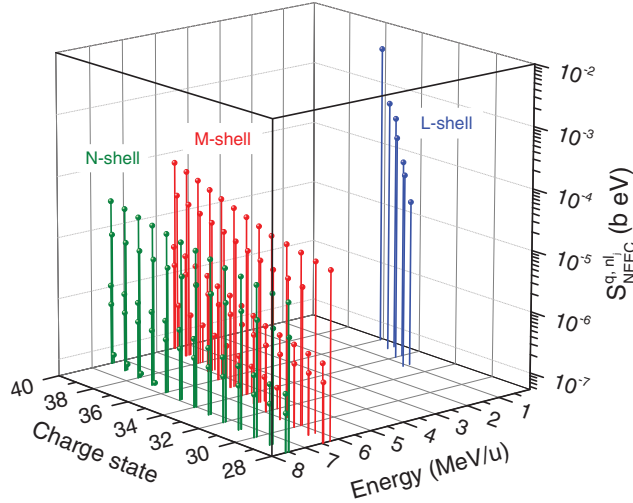


FIG. 2. NEEC resonance strength  $S_{\text{NEEC}}^{q,nl_j}$  for captures into  $L$ ,  $M$ , and  $N$  subshells as a function of the kinetic energy and charge state of  $^{93m}\text{Mo}$  ions.

the total width of the DS. The reduced transition probabilities from the DS and the corresponding nuclear level widths were taken from Ref. [34].

The ICCs were calculated for a neutral atom ( $^{93}\text{Mo}^{q=0}$ ) with the frozen orbital approximation based on Dirac-Fock calculations [35,36]. The coefficients for  $^{93m}\text{Mo}$  ions (up to  $q = 40$ ) were obtained from the linear (quadratic for  $ns_{1/2}$  orbitals) scaling dependence between ICCs and binding energies of a specific subshell  $nl_j$  for ions and neutral atoms. The binding energies for neutral atoms were taken from tables [37], while those for ions were calculated by means of the multiconfigurational Dirac-Fock method [38–41]. The final  $\alpha_{\text{IC}}^{q,nl_j}(\text{DS} \rightarrow \text{IS})$  obtained in this way can only be used for a fully ionized subshell. For partially ionized subshells these coefficients must be reduced in proportion to the number of available vacancies  $n_v$  for the specific  $q$  in a given subshell that can accommodate up to  $N$  electrons, i.e.,  $\alpha_{\text{IC}}^{q,nl_j}(\text{DS} \rightarrow \text{IS})n_v/N$  [23].

Figure 2 shows resonance strengths of NEEC for  $L$ ,  $M$ , and  $N$  subshells calculated as a function of the projectile energy and  $q$  of  $^{93m}\text{Mo}$  ions ( $28 \leq q \leq 40$ ). The range of charge states in the case of electron capture into the  $L$  shell is limited from below to  $q = 33$  if one assumes the  $L$ -shell vacancies are available only for  $q > 32$  and limited from above to  $q = 36$  ( $q = 35$  for  $2p_{1/2}$ ) due to the binding energy limit (4.85 keV). The NEEC resonance strengths increase for higher  $q$  as a result of an increase in binding energies. The highest values of resonance strengths occur for captures into the  $L$  shell. However, in the NEEC recombination theory, the contribution of the  $L$  shell to the total NEEC probability is strongly suppressed by a highly limited number of charge states with available  $L$ -shell vacancies for low projectile energies. As a result,

the contribution of the  $L$  shell to the whole NEEC process is many orders of magnitude smaller than those of higher shells [28].

Because of the interaction of ions with the bound target electrons, a correct model should reflect how the electron momentum distribution contributes to the resonant transfer process. The Compton profile is related to the momentum density of an electron in a given carbon atom orbital with momentum  $p$ . The Compton profile formula that was originally derived for analyzing the Compton scattering of x rays by bound target electrons [42,43] can be written as

$$J_i(Q) = \frac{1}{2} \int_Q^\infty p |\psi_{ni}(p)|^2 dp, \quad (3)$$

where  $\psi_{ni}(p)$  is the Fourier transform of the spatial wave function [44] and  $Q$  is the projection of the initial target electron momentum  $p$  along the incident projectile axis. In the rest frame of the ion, the momentum component of the target electron along the ion-projectile axis can be obtained from the conservation law:

$$Q = \sqrt{\frac{M_p}{2E_p}} (\Delta E'_{\text{exc}} + E_{\text{bin}}(^{12}\text{C}) - \frac{m_e}{M_p} E_p), \quad (4)$$

where  $\Delta E'_{\text{exc}} = \Delta E_{\text{exc}} - E_{\text{bin}}(^{93m}\text{Mo})$ ,  $\Delta E_{\text{exc}} = 4.85$  keV is the energy needed to excite the  $^{93}\text{Mo}$  nucleus from IS ( $21/2^+$ ) to DS ( $17/2^+$ ),  $E_{\text{bin}}(^{93m}\text{Mo})$  is the binding energy for the capture orbital in  $^{93}\text{Mo}$ ,  $E_{\text{bin}}(^{12}\text{C})$  is the binding energy of the target electron (can be neglected for low- $Z$  targets such as carbon),  $M_p$  and  $E_p$  are the projectile mass and energy, and  $m_e$  is electron mass.

Using the NEEC resonance strengths determined from Eq. (2) and Compton profiles implemented from Ref. [44], we have obtained the corresponding NEEC-RT cross sections ( $\sigma_{\text{NEEC-RT}}^{q,nl_j}$ ). The cross sections include the contributions from all target electrons. Figure 3 shows three groups of the NEEC-RT cross sections including electron transfer from the carbon target into the  $2p_{3/2}$ ,  $3p_{3/2}$ , and  $4p_{3/2}$  subshells of  $^{93m}\text{Mo}^{q+}$  ions as a function of the projectile energy. The  $np_{3/2}$  orbitals give the largest contribution to the total NEEC-RT cross section for all considered shells of  $^{93m}\text{Mo}$  ions. The energy positions of the NEEC-RT cross-section maxima and their peak values reflect the resonance (discrete) NEEC energies and strengths (see Figs. 2 and 3). The broadenings of the NEEC-RT cross-section structures reveal the momentum distributions of the carbon-target electrons. These features extend the contributions of specific orbitals into the NEEC-RT process over the entire projectile energy range. The broadening is particularly striking for  $2p_{3/2}$  orbitals of  $^{93m}\text{Mo}$  ions, significantly increasing their role in NEEC-RT in comparison with the recombination NEEC process. Similar considerations were performed for the resonance

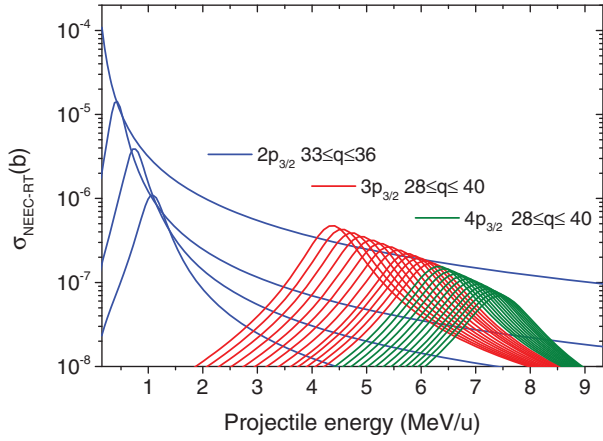


FIG. 3. NEEC-RT cross sections for the electron transfers from carbon target into  $2p_{3/2}$  (blue lines),  $3p_{3/2}$  (red lines), and  $4p_{3/2}$  subshells (green lines) of  $^{93m}\text{Mo}^{q+}$  ions as a function of the projectile energy. The topmost curve corresponds to the highest  $q$  for each subshell.

electron transfers into all considered subshells for which analogous conclusions may be formulated.

Next, we estimated the ion charge states appearing in different stages of the stopping process. Figure 4 shows charge-state distributions for  $^{93m}\text{Mo}$  ions colliding with a carbon target as a function of the projectile energy. The Gaussian distributions with width defined as  $d(\hat{q}) = [\sum_q (q - \hat{q})^2 F(q)]^{1/2}$  [45], where  $\hat{q}$  is an average charge state of  $^{93m}\text{Mo}$  ions, were employed for an estimation of the charge-state fractions. The mean equilibrium charge states were predicted by means of the Schiwietz and Grande formula [46], and widths of charge distributions from the formula of Nikolaev and Dmitriev [47]. In Ref. [28], different models of the mean charge state and distribution width, including the model we used in this work, were examined and found to produce similar results.

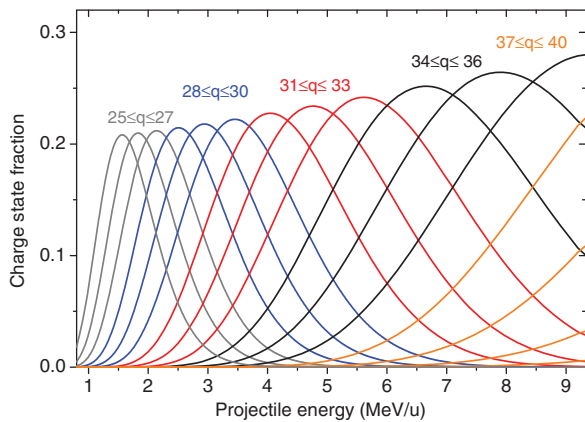


FIG. 4. Evolution of charge state fraction ( $f_q$ ) for  $^{93m}\text{Mo}$  ions colliding with carbon target as a function of the projectile energy.

After obtaining the NEEC-RT cross sections ( $\sigma_{\text{NEEC-RT}}$ ) and charge-state fractions ( $f_q$ ), we determined the  $^{93m}\text{Mo}$  isomer depletion function, i.e., the total sum of the products of the two (see Fig. 5). The total  $^{93m}\text{Mo}$  isomer depletion function has a two-hump structure corresponding to the maxima of the partial depletion functions for the  $M$  and  $N$  shells. One can also see a broad structure from the  $L$  shell giving a significant contribution to the total  $^{93m}\text{Mo}$  isomer depletion function. This is fundamentally different from the NEEC recombination model.

To determine the probability for the NEEC-RT process occurring in a  $^{93m}\text{Mo}$  ion interacting with a carbon target of thickness  $x$ , we used the relation

$$P_{\text{NEEC-RT}} = N(^{12}\text{C}) \sum_{q, n_l j} \int_{E_0}^0 f_q \sigma_{\text{NEEC-RT}}^{q, n_l j} \frac{dE}{dx} dE, \quad (5)$$

where  $E_0 = 9.33$  MeV/ $u$  is the upper limit for the  $^{93m}\text{Mo}$  ion energy taken as an initial preliminary beam energy used in the Argonne experiment (the mean energy of  $^{93m}\text{Mo}$  recoil ions produced in fusion-evaporation reactions was somewhat lower),  $dE/dx$  is the stopping power, and  $N(^{12}\text{C})$  is the  $^{12}\text{C}$  target atom density. The stopping power as a function of energy of  $^{93m}\text{Mo}$  ions interacting with a carbon target were determined using the CASP code [48,49]. We employed the unitary convolution approximation with shell, binding, and the projectile nuclear charge screening corrections.

Our theoretical predictions for the total and partial (for  $L$ ,  $M$ , and  $N$  shells) probabilities of the NEEC-RT process for the  $^{93m}\text{Mo}$  isomer are presented in Table I. Previous theoretical predictions based on the recombination

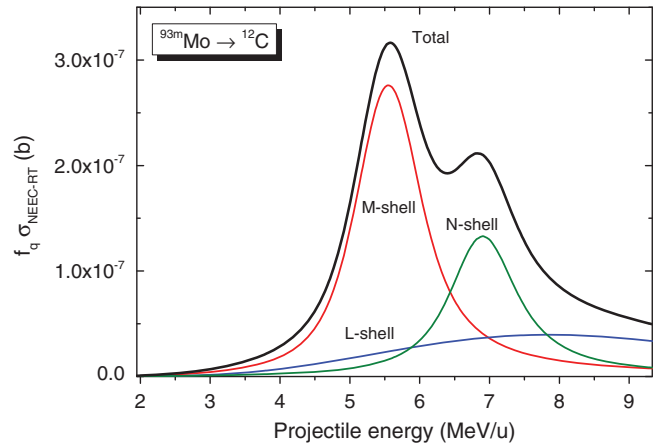


FIG. 5. The  $^{93m}\text{Mo}$  isomer depletion function (sum of the products of the NEEC-RT cross sections and charge-state fractions) including the electron transfer from a carbon target into  $L$  (blue line),  $M$  (red line), and  $N$  (green line) shells of  $^{93m}\text{Mo}^{q+}$  ( $28 \leq q \leq 40$ ) ions and the total depletion function (black line) as a function of the projectile energy.

TABLE I. Partial and total probabilities for  $^{93m}\text{Mo}$  isomer depletion as a result of the electron capture into  $L$ ,  $M$ , and  $N$  shells of the ion projectile.

|                         | $L$ shell              | $M$ shell              | $N$ shell              | Total ( $L + M + N$ )   |
|-------------------------|------------------------|------------------------|------------------------|-------------------------|
| Model (i) <sup>a</sup>  | $5.68 \times 10^{-18}$ | $1.53 \times 10^{-11}$ | $7.54 \times 10^{-12}$ | $2.28 \times 10^{-11}$  |
| Model (ii) <sup>a</sup> | $1.48 \times 10^{-19}$ | $1.47 \times 10^{-11}$ | $7.34 \times 10^{-12}$ | $2.20 \times 10^{-11}$  |
| Present                 | $1.49 \times 10^{-11}$ | $3.58 \times 10^{-11}$ | $1.90 \times 10^{-11}$ | $6.98 \times 10^{-11}$  |
| Experiment <sup>b</sup> |                        |                        |                        | $1.0(3) \times 10^{-2}$ |

<sup>a</sup>Wu *et al.* [28].

<sup>b</sup>Chiara *et al.* [26].

NEEC approach with two different models of  $^{93m}\text{Mo}$  mean ion charge states [28] and the experimental value [26] are also shown.

The NEEC-RT probability we obtained for the  $L$  shell is many orders of magnitude higher than that obtained from the previous predictions [28]. In the case of  $M$  and  $N$  shells, the increase in NEEC-RT probabilities is much weaker. To recognize what part of the gain is due to the recombination model difference and what part is from the Compton profile effect itself, we estimated the recombination NEEC probabilities on the basis of our NEEC resonance strengths (as described above and in Ref. [23]) and exactly the same ion charge distributions and stopping power calculations as those used in Ref. [28].

The absolute values obtained in our recombination estimation are higher for the  $M$  and  $N$  shell by a factor of 2.4–2.7, and a factor of 1.1 or 43.9 for the  $L$  shell depending on the model, with respect to the NEEC recombination probabilities obtained in Ref. [28]. Although the understanding of the observed differences between our and Wu *et al.*'s recombination models requires further research, one essential point can be clearly stated: taking into account the Compton profile greatly enhances the NEEC probability for the  $L$  shell of  $^{93m}\text{Mo}$  ions, while there is no enhancement for  $M$  and  $N$  shells. The exceptionally large enhancement for the  $L$  shell is the result of the extremely wide structure of the isomer depletion function, thanks to which all ion charge states can contribute to the NEEC-RT process even for ground-state atomic configurations. This feature restores the important role of the  $L$  shell in the isomer depletion process which is suppressed by many orders of magnitude in the recombination models. The probability obtained for the  $L$  shell from the resonant transfer (NEEC-RT) approach, being 6–8 orders of magnitude larger than those obtained from the NEEC recombination models, most clearly shows the fundamental difference between the resonant transfer and recombination approaches. Thus, the probability for the  $L$  shell gives a comparable contribution to the total NEEC-RT probability as that of  $M$  and  $N$  shells and in this way raises the upper theoretical limit for the isomer depletion. The interesting role of the  $L$  shell is also suggested by the large difference for the  $L$  shell between the models of Wu *et al.*, and by the

apparent suppression of the contribution of the  $L$  shell to the depletion probability for ground-state configurations. Including excited-state configurations in the future model can further enhance the role of the  $L$  shell of the  $^{93m}\text{Mo}$  ions in the NEEC-RT process [50]. Note in Fig. 4 that the mean charge distribution for a ground-state configuration gives  $f_q \sim 0$  near 1 MeV/ $u$  for the  $L$  shell. Even a small but non-negligible effective  $f_q$  for the  $L$  shell, due to excited-state configurations, would tap into the extremely large NEEC-RT cross section at that energy.

In summary, a novel theoretical approach for isomer depletion in beam-based conditions has been proposed. We considered the  $^{93m}\text{Mo}$  isomer excitation as a result of the resonant electron transfer from the carbon target into highly charged  $^{93m}\text{Mo}$  ions taking into account the Compton profile of target electrons. Our analyses provided information on the shape of the  $^{93m}\text{Mo}$  isomer depletion function. The exceptionally large role of the  $L$  shell of the  $^{93m}\text{Mo}$  ions in the NEEC-RT process has been shown. New predictions for the probability of the  $^{93m}\text{Mo}$  isomer depletion based on the resonant transfer approach slightly move the upper theoretical limit toward the still distant experimental value.

This work is supported by the National Science Centre, Poland under Grant No. 2017/25/B/ST2/00901.

*Note added.*—Recently, we found a paper which attempted to note the distinction that in NEEC-RT, the ion captures an initially bound electron, while in NEEC, the electron is unbound [51].

\*Corresponding author.

jacek.rzadkiewicz@ncbj.gov.pl

- [1] G. D. Dracoulis, P. M. Walker, and F. G. Kondev, *Rep. Prog. Phys.* **79**, 076301 (2016).
- [2] P. M. Walker and G. D. Dracoulis, *Nature (London)* **399**, 35 (1999).
- [3] D. Belic *et al.*, *Phys. Rev. Lett.* **83**, 5242 (1999).
- [4] G. D. Dracoulis, F. G. Kondev, G. J. Lane, A. P. Byrne, M. P. Carpenter, R. V. F. Janssens, T. Lauritsen, C. J. Lister, D. Seweryniak, and P. Chowdhury, *Phys. Rev. C* **81**, 011301(R) (2010).

- [5] J. J. Carroll, *Nucl. Instrum. Methods Phys. Res., Sect. B* **261**, 960 (2007).
- [6] J. J. Carroll, Nuclear metastables for energy and power: Status and challenges, in *Innovations in Army Energy and Power Materials Technologies*, edited by E. C. Shaffer and T. S. Zheleva (Materials Research Forum, Millersville, PA, 2018).
- [7] J. J. Carroll, M. S. Litz, K. A. Netherton, S. L. Henriquez, N. R. Pereira, D. A. Burns, and S. A. Karamian, *AIP Conf. Proc.* **1525**, 586 (2013).
- [8] A. A. Zadernovsky and J. J. Carroll, *Hyperfine Interact.* **143**, 153 (2002).
- [9] M. R. Harston and J. J. Carroll, *Laser Phys.* **15**, 487 (2005).
- [10] V. I. Goldanskii and V. A. Namiot, *Phys. Lett.* **62B**, 393 (1976).
- [11] M. R. Harston and J. F. Chemin, *Phys. Rev. C* **59**, 2462 (1999).
- [12] G. Gosselin, V. Méot, and P. Morel, *Phys. Rev. C* **76**, 044611 (2007).
- [13] J. Gunst, Y. A. Litvinov, C. H. Keitel, and A. Pálffy, *Phys. Rev. Lett.* **112**, 082501 (2014).
- [14] Y. Wu, J. Gunst, C. H. Keitel, and A. Pálffy, *Phys. Rev. Lett.* **120**, 052504 (2018).
- [15] L. Bernstein, EBIT plans in Livermore and Berkeley, at the *ECT\* Workshop on Atomic Effects in Nuclear Excitation and Decay, Trento, Italy, 2009*.
- [16] A. Pálffy, Z. Harman, C. Kozhuharov, C. Brandau, C. H. Keitel, W. Scheid, and T. Stöhlker, *Phys. Lett. B* **661**, 330 (2008).
- [17] A. Pálffy, W. Scheid, and Z. Harman, *Phys. Rev. A* **73**, 012715 (2006).
- [18] P. Morel, J. M. Daugas, G. Gosselin, V. Méot, and D. Gogny, *AIP Conf. Proc.* **769**, 1085 (2005).
- [19] N. Cue, J.-C. Poizat, and J. Remillieux, *Europhys. Lett.* **8**, 19 (1989).
- [20] Z.-S. Yuan and J. C. Kimball, *Phys. Rev. C* **47**, 323 (1993).
- [21] S. A. Karamian and J. J. Carroll, *Phys. At. Nucl.* **75**, 1362 (2012).
- [22] M. Polasik, K. Słabkowska, J. J. Carroll, C. J. Chiara, Ł. Syrocki, E. Węder, and J. Rządiewicz, *Phys. Rev. C* **95**, 034312 (2017).
- [23] J. Rządiewicz, M. Polasik, K. Słabkowska, Ł. Syrocki, E. Węder, J. J. Carroll, and C. J. Chiara, *Phys. Rev. C* **99**, 044309 (2019).
- [24] Ł. Syrocki, E. Węder, K. Słabkowska, M. Polasik, J. Rządiewicz, J. J. Carroll, and C. J. Chiara, *Acta Phys. Pol. B* **50**, 1359 (2019).
- [25] K. Słabkowska, E. Węder, Ł. Syrocki, M. Polasik, J. Rządiewicz, J. J. Carroll, and C. J. Chiara, *Acta Phys. Pol. B* **50**, 651 (2019).
- [26] C. J. Chiara, J. J. Carroll, M. P. Carpenter, J. P. Greene, D. J. Hartley, R. V. F. Janssens, G. J. Lane, J. C. Marsh, D. A. Matterns, M. Polasik, J. Rządiewicz, D. Seweryniak, S. Zhu, S. Bottoni, A. B. Hayes, and S. A. Karamian, *Nature (London)* **554**, 216 (2018).
- [27] C. M. Baglin, *Nucl. Data Sheets* **112**, 1163 (2011).
- [28] Y. Wu, C. H. Keitel, and A. Pálffy, *Phys. Rev. Lett.* **122**, 212501 (2019).
- [29] J. A. Tanis, E. M. Bernstein, W. G. Graham, M. P. Stockli, M. Clark, R. H. McFarland, T. J. Morgan, K. H. Berkner, A. S. Schlachter, and J. W. Stearns, *Phys. Rev. Lett.* **53**, 2551 (1984).
- [30] W. G. Graham, K. H. Berkner, E. M. Bernstein, M. W. Clark, B. Feinberg, M. A. McMahan, T. J. Morgan, W. Rathbun, A. S. Schlachter, and J. A. Tanis, *Phys. Rev. Lett.* **65**, 2773 (1990).
- [31] X. Ma, P. H. Mokler, F. Bosch, A. Gumberidze, C. Kozhuharov, D. Liesen, D. Sierpowski, Z. Stachura, T. Stöhlker, and A. Warczak, *Phys. Rev. A* **68**, 042712 (2003).
- [32] H. Xiao-Li, Q. Yi-Zhi, Z. Song-Bin, and Z. Yu, *Chin. Phys. B* **21**, 103401 (2012).
- [33] D. Brandt, *Phys. Rev. A* **27**, 1314 (1983).
- [34] M. Hasegawa, Y. Sun, S. Tazaki, K. Kaneko, and T. Mizusaki, *Phys. Lett. B* **696**, 197 (2011).
- [35] S. Raman, C. W. Nestor Jr., A. Ichihara, and M. B. Trzhaskovskaya, *Phys. Rev. C* **66**, 044312 (2002).
- [36] T. Kibédi, T. W. Burrows, M. B. Trzhaskovskaya, P. M. Davidson, and C. W. Nestor Jr., *Nucl. Instrum. Methods Phys. Res., Sect. A* **589**, 202 (2008).
- [37] F. B. Larkins, *At. Data Nucl. Data Tables* **20**, 311 (1977).
- [38] I. P. Grant and H. M. Quiney, *Adv. At. Mol. Phys.* **23**, 37 (1988).
- [39] K. G. Dylla, I. P. Grant, C. T. Johnson, F. A. Parpia, and E. P. Plummer, *Comput. Phys. Commun.* **55**, 425 (1989).
- [40] M. Polasik, *Phys. Rev. A* **39**, 616 (1989); **39**, 5092 (1989); **40**, 4361 (1989); **41**, 3689 (1990); **52**, 227 (1995).
- [41] M. Polasik, K. Słabkowska, J. Rządiewicz, K. Koziół, J. Starosta, E. Wiatrowska-Koziół, J. C. Dousse, and J. Hoszowska, *Phys. Rev. Lett.* **107**, 073001 (2011).
- [42] P. Eisenberger and P. M. Platzman, *Phys. Rev. A* **2**, 415 (1970).
- [43] P. Eisenberger and W. A. Reed, *Phys. Rev. A* **5**, 2085 (1972).
- [44] F. Biggs, L. B. Mendelsohn, and J. B. Mann, *At. Data Nucl. Data Tables* **16**, 201 (1975).
- [45] H.-D. Betz, *Rev. Mod. Phys.* **44**, 465 (1972).
- [46] G. Schiwietz and P. L. Grande, *Nucl. Instrum. Methods Phys. Res., Sect. B* **175–177**, 125 (2001).
- [47] V. S. Nikolaev and I. S. Dmitriev, *Phys. Lett. A* **28**, 277 (1968).
- [48] CASP website, [https://www.helmholtz-berlin.de/people/gregor-schiwietz/casp\\_en.html](https://www.helmholtz-berlin.de/people/gregor-schiwietz/casp_en.html) (2020).
- [49] G. Schiwietz and P. L. Grande, *Phys. Rev. A* **84**, 052703 (2011).
- [50] S. Gargiulo, I. Madan, and F. Carbone, arXiv:2102.05718.
- [51] T. Mukoyama, *AIP Conf. Proc.* **652**, 281 (2003).